NJC

Accepted Manuscript

This is an *Accepted Manuscript*, which has been through the Royal Society of Chemistry peer review process and has been accepted for publication.

Accepted Manuscripts are published online shortly after acceptance, before technical editing, formatting and proof reading. Using this free service, authors can make their results available to the community, in citable form, before we publish the edited article. We will replace this *Accepted Manuscript* with the edited and formatted *Advance Article* as soon as it is available.

You can find more information about *Accepted Manuscripts* in the Information for Authors.

Please note that technical editing may introduce minor changes to the text and/or graphics, which may alter content. The journal's standard Terms & Conditions and the Ethical guidelines still apply. In no event shall the Royal Society of Chemistry be held responsible for any errors or omissions in this *Accepted Manuscript* or any consequences arising from the use of any information it contains.

ROYAL SOCIETY OF CHEMISTRY

www.rsc.org/njc

Radiolytic Synthesis of Au-Cu Bimetallic Nanoparticles Supported on TiO_2: Application in Photocatalysis

Zibin Hai[1,2,3], Nadia EL Kolli[1], Jiafu Chen[2] and Hynd Remita[1,4*]

[1]Laboratoire de Chimie Physique, CNRS - UMR 8000, Université Paris-Sud, 91405 Orsay, France
[2]Hefei National Laboratory for Physical Sciences at the Microscale, University of Science and Technology of China, Hefei, Anhui 230026, China
[3]Anhui Academy of Environmental Science Research, Hefei, Anhui 230071, China
[4]CNRS, Laboratoire de Chimie Physique, UMR 8000, 91405 Orsay, France

Abstract

Modification of TiO_2 (P25) with Au-Cu bimetallic nanoparticles (NPs) was successfully achieved via deposition precipitation method with urea (DPU) followed by radiolytic reduction. This deposition procedure ensures a complete adsorption of Au and Cu ions on TiO_2. Small Au-Cu NPs homogeneous in size were obtained. The alloyed structure of Au-Cu NPs was confirmed by HAADF-STEM, EDS, HRTEM and XPS techniques. The photocatalytic properties of the modified TiO_2 have been studied for photodegradation of methyl orange. The modification with Au-Cu bimetallic nanoparticles induces an enhancement in the photocatalytic activity under UV irradiation. The highest photocatalytic activity was obtained with Au-Cu/TiO_2 (Au/Cu = 1:3). Bimetallic Au-Cu NPs act as efficient electron scavengers increasing the photocatalytic activity under UV light.

1 Introduction

Titania (titanium (IV) dioxide, TiO_2) has been extensively studied for decades because of its photocatalytic properties, excellent resistance to photocorrosion, non-toxicity and low cost. TiO_2 exists in nature in three crystallographic phases: anatase, rutile and brookite. Among them, anatase and rutile are the most commonly phases used in photocatalysis, their band-gap energy are 3.2 eV and 3.0 eV respectively. The limitation in titania application results from its low quantum yield of solar energy conversion due to the fast charge carrier recombination and the necessity to use UV irradiation. Indeed, TiO_2 absorbs only 3-4 % of the solar illumination deposited on the Earth's surface as it can be excited only under UV light with wavelengths

shorter than 400 nm. Moreover, as in most of semiconductors, a high rate of electron-hole recombination results in low quantum yield. To enhance the photocatalytic activity of TiO_2, its modification is in general involved.[1, 2]

Degussa P25 (a commercial TiO_2, is a mixture of 80% of anatase and 20% of rutile) is very photoactive under UV light due to its anatase-rutile junction decreasing the recombination rate of photoinduced electron-hole pairs.[3] It has been reported that the photocatalytic activity of TiO_2 (especially anatase) can be improved by surface modification with metal nanoparticles especially with noble metals such as Pt, Pd, Ir, Ag and Au.[4-19] However, there are few works focused on modification of TiO_2 or other supports with Cu.[20-22] Some non-noble metals such as Cu have excellent catalytic properties but they are not stable at nano-scale size. Only a few studies report on modification of titania with bimetallic Au-Cu nanoparticles.[19, 23-26] Bimetallic nanomaterials have attracted much attention because of their potential application in various technologically important fields due to their unique catalytic, electrocatalytic, electronic and magnetic properties, which differ from their monometallic counterparts. Bimetallic nanoparticles often exhibit enhanced catalytic performances in terms of activity, selectivity and stability, compared to the separate components.[23-25, 27, 28] For example, bimetallic Au–Cu on TiO_2 are more active and selective towards propene epoxidation by nitrous oxide than monometallic Au or Cu samples supported on TiO_2.[23] Recently, it has been shown that Au–Cu bimetallic nanoparticles exhibit higher catalytic activities than monometallic gold catalysts, for both CO oxidation and PROX reactions.[24, 25] In the field of electrocatalysis, carbon electrodes modified with bimetallic Au-Cu NPs were found promising for electrocatalytic oxidation of glucose in alkaline solution.[29]

Here, we modified the surface of commercial P25 TiO_2 by bimetallic Au-Cu nanoparticles using deposition-precipitation with urea (DPU method) followed by radiolytic reduction. The modified Au-Cu/P25 photocatalysts were studied for photodegradation of methyl orange under UV and visible illumination.

2 Experimental Section

2.1 Materials

All the reagents were used without further purification. *Titanium dioxide* (TiO_2, Evonik P25, 50 m^2g^{-1}, 80% of Anatase, 20% of Rutile) was purchased from *Evonik*, Germany. Chloroauric

Acid (HAuCl4, 3H2O), *Copper Chloride Dihydrate* ($CuCl_2$, $2H_2O$), and Methyl Orange ($C_{14}H_{14}N_3SO_3Na$) were purchased from *Sinopharm* Chemical Reagent Co., Ltd. Deionized water (Milli Q with 18.6 MΩ•cm) was used all through this work.

2.2 Preparation of the photocatalysts

A typical synthesis of bimetallic Au-Cu NPs modified P25 at a total metal content of 0.5 wt. % is described as below. 0.478 mL of $HAuCl_4$ solution (10^{-2} M) was added to a flask of 25 mL of distilled water. 250 mg of P25 and 37.5 mg of urea were added to the solution to form a white suspension. The flask was then heated up to 90 °C in a water bath under stirring. The temperature of water bath was kept at 90 °C for 2 hours. At this point, the well dispersed suspension turned into a well formed precipitate. 0.478 mL of an aqueous solution of $CuCl_2$ (10^{-2} M) was added into the flask. The temperature decreased naturally to room temperature with keeping magnetic stirring. 0.192 mL of 2-propanol was then added to the suspensions (to scavenge the oxidative $OH^{\bullet}$ radicals generated during γ-irradiation of water), which were first degassed with N_2 and then irradiated for 3 hours (under stirring) with a ^{60}Co panoramic gamma source (dose rate = 10 $kGy.h^{-1}$). The metal ions (Au^{III} and Cu^{II}) were reduced by the solvated electrons and the alcohol radicals induced by solvent radiolysis. After irradiation, the white suspension turned to violet. The modified TiO_2 photocatalysts were separated by centrifugation, washed several times with deionized water and then dried in air at 50 °C. Violet powders were obtained.

2.3 Characterization of the modified TiO_2

UV−visible diffuse reflectance spectra of the photocatalysts were recorded using a Shimadzu DUV3700 spectrophotometer in the region of 200 to 800 nm. X-ray photoelectron spectroscopy (XPS) analysis was performed on a Perkin-Elmer RBD upgraded PHI-5000C ESCA system. Sample drops were deposited on In foils and dried under N_2 flow.

High angle annular dark field (HAADF) scanning transmission electron microscopy (STEM) was conducted with a JEM 2100F microscope. Energy dispersive X-ray (EDX) mapping was recorded with an X-Max Silicon Drift Detector (SDD) from Oxford.

N_2 adsorption isotherms were performed by BET measurements using a Tristar II 3020M surface area analyzer. Brunauer-Emmett-Teller (BET) surface area was determined by a

multipoint BET method in the relative pressure (P/P_0) rang of 0.07-0.2.

Photoluminescence spectra were recorded with a JY Fluorolog-3-Tou fluorescence spectrophotometer with an exciting wavelength of 350 nm.

2.4 Photocatalytic reactions

Methyl orange (MO) was used as a model pollutant. It is a representative of a hazardous azo dye. The photocatalytic experiments were carried out in a XPA-7 photochemical reactor (Nanjing Xujiang Machine-electronic Plant, China). The detailed description of the reactor apparatus can be found in **Figure S1**.

For the photocatalytic reactions under UV illumination, a 300 W mercury lamp was used as the light source. Optical filters were employed to cut off the unwanted light. For UV irradiations, a filter was used to allow only the illumination at wavelengths larger than 270 nm and shorter than 400 nm.

Typically, 20 mg of the synthesized photocatalyst was dispersed in 20 mL of a solution of methyl orange (MO) with a concentration of 20 mg L^{-1}. The suspension was put in a silica tube, followed by ultra-sonication for 30 seconds to disperse the powder. The solution was then kept under stirring in dark for 30 minutes to reach the equilibrium between adsorption and desorption of MO on the surface of photocatalysts. The slurry was then subjected to UV irradiation under magnetic stirring and oxygen bubbling (flow rate of 200 mL min^{-1}). 2 mL aliquots were taken from the reactor at fixed time intervals. The suspensions were centrifuged at 4000 rpm for 20 minutes to obtain clear supernatants. For the photocatalytic tests under visible irradiation, a 500 W Xenon lamp was used as the light source, equipped with another optical filter cutting wavelengths shorter than 450 nm.

The MO solutions and the supernatants (after the photocatalytic reactions) were analyzed using a Shimadzu UV-1800 UV-Visible spectrophotometer.

3 Results and Discussion

3.1 Deposition by DPU method of Au and/or Cu ions on P25 and radiolytic reduction

Deposition-precipitation with urea (DPU) was developed on the basis of deposition-precipitation with NaOH initiated by Haruta.[30, 31] In the DPU method, the metal precursors are mixed with the supports forming an aqueous suspension, subsequently

precipitated as a hydroxide by increasing the pH value. The key point of the DP is the prevention of precipitation away from the surface of the supports. Louis and Zanella *et al*. synthesized Au, Pd and other noble metal nanoparticles supported on TiO_2 and Al_2O_3 with DPU method,[32-35] followed by H_2 reduction. Here, we report synthesis of bimetallic Au-Cu nanoparticles supported on TiO_2 by a DPU method, introducing the metal ions to the suspension in two steps followed by radiolytic reduction.

After deposition of Cu, Au and Cu-Au on P25 by DPU method, the samples were irradiated for reduction of the deposited Au^{III} and Cu^{II} ions. The resulting modified monometallic catalysts were Au on P25 (referred as Au/P25) and Cu on P25 (referred as Cu/P25) (0.5 wt% of metal on TiO_2). Correspondingly, AuCu1:1/P25 represents the sample P25 modified with Au-Cu NPs with an Au/Cu molar ratio of 1:1. The total nominal metal content was kept at 0.5 wt%. The compositions of the modified P25 by DPU are listed in details in **Table 1**.

Table 1 The conditions and compositions of the Au, Cu, and Au-Cu modified P25 by Deposition Precipitation with Urea.

Photocatalyst	Molar Ratio of Au/Cu	Content of metal precursor/P25 (wt %)		Color	[a]mean size (nm) (from TEM pictures)
		Au	Cu		
Au/P25	1:0	0.5	0	Violet	8.4
AuCu1:1/P25	1:1	0.38	0.12	Light-violet	8.2
AuCu1:3/P25	1:3	0.25	0.25	Grey-violet	6.4
Cu/P25	0:1	0	0.5	Light-green	[b]N/A

[a]Mean size: measured manually with a program (Nano measurement);

[b]N/A:In case of Cu on TiO_2, we did not observe any metal nanoparticle on the support.

In order to evaluate the deposition efficiency of the Au-Cu ions with the DPU method, the supernatants of the mixture were monitored using UV-vis absorption spectrophotometer. Typically, the spectrum of AuCu1:1/P25 supernatant before irradiation (**Figure S2**, trace **a**) shows no absorption peaks in the UV-visible region except for a peak at around 200 nm, which is attributed to urea in the solution. This illustrates that the $[AuCl_4]^-$ and Cu^{2+} are not present in the supernatant, namely they completely deposited on the surface of TiO_2. The

spectrum of AuCu1:1/P25 after irradiation was almost the same as that before irradiation except for the small absorption peak at 262 nm. We assumed that this small peak was due to the instrinsic absorption of TiO_2 in the UV region. This was confirmed by UV-Vis absorption spectra of the supernatant along with filtration cycling.

The first chemical step occurred during DPU preparation of Au on TiO_2 is the formation of surface complexes. The surface complex $AuCl_3(OH)^-$ links to the TiO_2 surface by the interaction with surface OH to form Ti-O-$AuCl_2$ instead of an electrostatic attraction.[36] Furthermore, the other negative gold complexes $AuCl(OH)_3^-$, $AuCl_2(OH)_2^-$ and $AuCl_3(OH)^-$ can also link to the TiO_2 surface. In the case of DPU, the adsorption of gold hydroxy chlorides on TiO_2 increased as pH increased, meaning more and more OH were generated in this process. The pH was slightly higher (~6.5) than PZC_{TiO2} (point of zero charge, PZC_{TiO2} ~ 6.3) after the complete deposition. Thus, the surface of TiO_2 was negatively charged. Cu^{2+} was introduced in a second step into the suspension and was adsorbed on the TiO_2 surface.

Considering that TiO_2 is an amphoteric oxide, a colloidal TiO_2 suspension just could be formed when the solution pH is less than 6. Before irradiation, the solution was nearly neutral. Gamma irradiation leads to pH decrease because water radiolysis induces the formation of H^+. In this case, TiO_2 particles can be easily separated by centrifugation. After gamma irradiation, when the pH value decreased below PZC_{TiO2}, it was impossible to remove the tinny particles by centrifugation. The supernatent spectrum indicates that all the Au and Cu ions were efficiently deposited on TiO_2. For the other prepared mono- and bimetallic modified photocatalysts, similar results obtained are shown in **Figure S3-S6**.

In the absence of urea, residual Au^{III} complexes can be detected from the UV-Vis spectra of the supernatant of sample Au/P25 (**Figure S7**). In this case, the metal ion deposition was not efficient and the size of metal NPs induced by radiolysis and deposited on P25 was much larger compared to that prepared by deposition precipitation method with urea (**Figure S8**).

Au^{III} and Cu^{II} ions deposited on TiO_2 were reduced by solvated electrons and reducing $(CH_3)_2C^{\bullet}OH$ radicals induced by solvent radiolysis.[37-39] Indeed, high energy radiation (γ-rays, X-rays, electrons or ions beams) of water leads to the formation of free radicals such as solvated electrons (e^-_s) (which are strong reducing species) and $H^{\bullet}$ and $OH^{\bullet}$ radicals. Oxidation by hydroxyl radical $OH^{\bullet}$ is avoided by addition of radical scavengers, such as

2-propanol, which yields after reactions with $OH^{\bullet}$ and $H^{\bullet}$ to a secondary reducing radical $(CH_3)_2C^{\bullet}OH$. Solvated electrons e^-_s and alcohol radicals are strong reducing agents able to reduce metal ions to lower valences and finally to metal atoms. The energy deposition throughout the solution ensures an initial homogeneous distribution of the radiolytic radicals and therefore a homogeneous reduction and nucleation.[37, 38]

3.2 Characterization of the modified TiO_2

3.2.1 TEM Characterization

TEM images show well distibuted metal nanoparticles (monometallic Au or bimetallic Au-Cu NPs) on TiO_2 (**Figure 1α,c,e**). The size of the metal NPs decreased slightly with the increase of Cu proportion in the bimetallic NPs: for monometallic Au NPs on P25, the mean size was around 8.4 nm, for AuCu1:3/P25, the mean size was around 6.4 nm (see **Table 1**). It has been already reported that the size of Au-Cu alloyed NPs decreased with increasing the amount of Cu in the bimetallic NPs.[24] In the case of monometallic Cu NPs on TiO_2, no particles could be observed on the TiO_2 support, probably because of the small size of Cu clusters and the small contrast between copper and titianium (the images are not shown).

The supported monometallic Au and bimetallic Au-Cu NPs were observed by HRTEM. **Figure 1b** shows HRTEM images of the sample Au/P25. The interplanar crystal spacing is 0.238 nm from the lattice fringes. This value corresponds to the interplanar crystal spacing of Au(111) (0.235 nm from the JCPDS-PDF 04-0784). For the sample AuCu1:1/P25 (**Figure 1d**), the interplanar crystal spacing of the supported nanoparticlesis 0.227 nm. According to the Vegard's law, we could get the theoretical value of 0.221 nm for the (111) lattice planes for alloyed Au/Cu1:1 NPs. In the case of the sample AuCu1:3/P25, the spacing value of the Au-Cu bimetallic nanoparticles on P25 is smaller (0.218 nm, **Figure 1f**), indicating a higher proportion of Cu in the bimetallic Au-Cu NPs. The HRTEM results probably evidenced the alloyed bimetallic nanostructure for the supported Au-Cu NPs on P25. However, it should also be pointed out that the Vegard's law is not necessarily followed by nanoalloys.

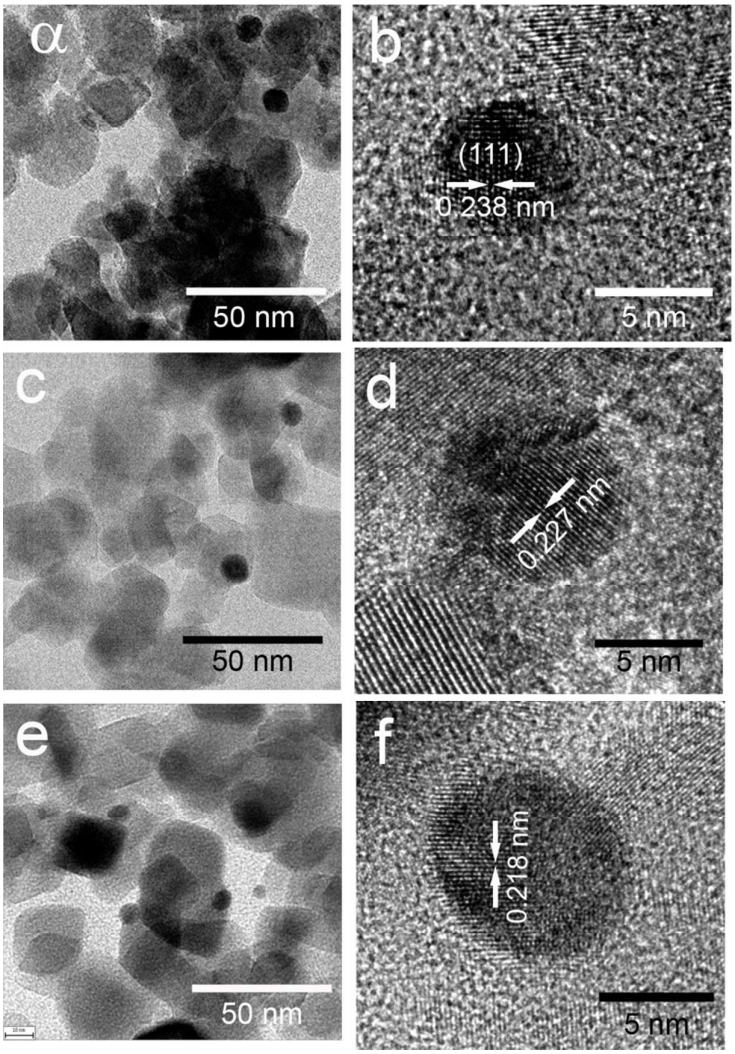

Figure 1 TEM images of (α) Au/P25, (c) AuCu1:1/P25, (e) AuCu1:3/P25; HR-TEM images of (b) Au/P25, (d) AuCu1:1/P25, and (f) AuCu1:3/P25. Dose rate: 170 Gy min^{-1}, dose: 30 kGy.

3.2.2 EDS Analysis

The composition of the Au-Cu nanoparticles on P25 was determined by STEM-Electron dispersive X-ray spectroscopy (EDS). EDS profile scans were carried out across different Au-Cu NPs. For the sample AuCu1:1/P25, a representative nanoparticle is shown in **Figure 2**. The Au-Lα1 and Cu-Kα1 line scan signals showed clearly the same intensity along the different regions of the NPs, implying that the Au and Cu atoms are approximately homogeneously distributed. Therefore, the EDS profile scans evidenced the alloyed structure of bimetallic Au-Cu NPs. Because of the low diffraction capability of Cu, the Cu signal is much lower than that of Au. Indeed, the atomic ratio of Au to Cu was around 1:2 from the

EDS spectrum, deviated from the nominal ratio of 1:1. Furthermore, EDS elemental mapping was also attempted to detect respective elements (**Figure 2**, bottom). AuLα1 and CuKα1 maps clearly identified the alloyed structure of the Au-Cu bimetallic NPs. Similar HAADF-STEM images and EDS results were obtained on different nanoparticles indicating that Au-Cu nanoparticles homogeneous in size, compositions and structure were synthesized on TiO_2.

HR-TEM images and EDS analyses show that the supported bimetallic Au-Cu NPs on P25 are nanoalloys.

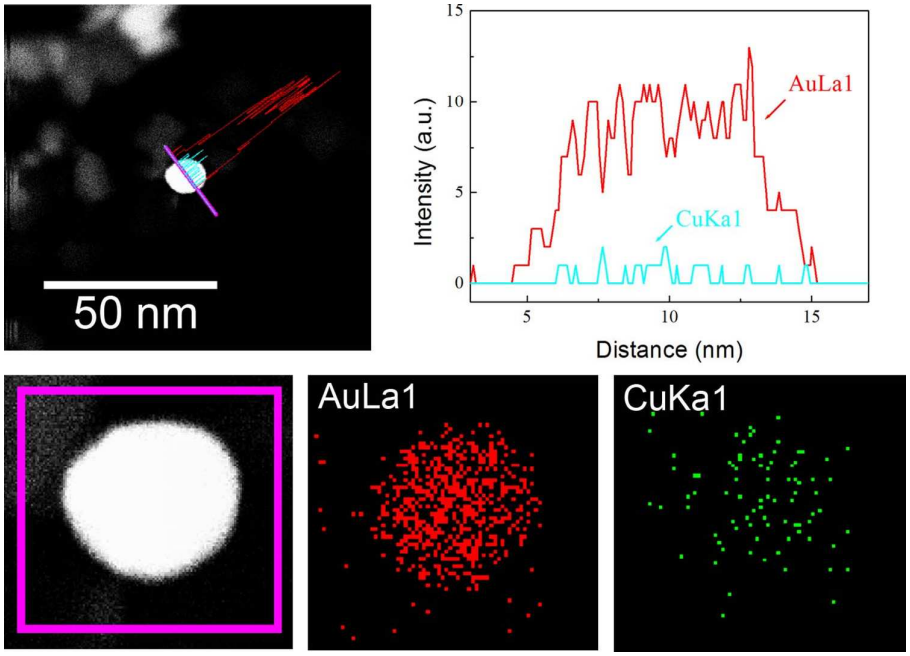

Figure 2, Top. HAADF-STEM image of AuCu1:1/P25 (left) and the corresponding Energy Dispersive X-ray Spectroscopy line scan across an AuCu1:1 NPs (right. The profile was taken along the purple line; the blue line corresponds to CuK and the red one to AuL signal). **Bottom**. Mapping EDS analysis performed for an Au/Cu1:1 nanoparticle.

3.2.3 BET Analysis

Nitrogen sorption isotherms were generated to investigate the porous structure and the Brunauer-Emmett-Teller (BET) surface areas of the modified photocatalysts. The results are discussed in **SI** and the data are shown in **Figure S9**. The BET surface area was obtained as 47.0 $m^2 g^{-1}$. Compared to the reference P25 (51.4 $m^2 g^{-1}$), a slight decrease in the BET surface area was found.

3.2.4 XPS Analysis

In order to analyze the chemical composition of the modified TiO_2 and to identify the chemical status of Cu element in the samples, X-ray photoelectron spectroscopy (XPS) measurements were attempted. The XPS survey spectrum of AuCu1:3/P25 is shown in **Figure 3a**. The peaks of Cu2p, Au4f, Ti2p, O1s, and C1s can be clearly detected. The weak peaks of C are contamination peaks arising mainly from CO_2 adsorbed on the surface of the sample. The high resolution XPS spectra of Cu in the region 2p and of Au in 4f for the sample AuCu1:3/P25 are shown in **Figure 3b** and **Figure S10**, respectively. The $Au4f_{7/2}$ core levels present their BE in the range 83.0 eV, so slightly negatively shifted compared to standard bare Au (84 eV). The position range is in agreement with the Au(0) chemical state but with a specific low BE position which has been already reported in the literature.[40,41] This shift can reflect the strong interaction of gold-based NPs with TiO_2 changing its electronic environment. Cu LMM and the Auger parameters were used to study the oxidation states of Cu-based nanoparticles.[42-44] The binding energies of $Cu2p_{3/2}$ and $Cu2p_{1/2}$ peaks are located at 931.7 and 951.5 eV, respectively, which agree with those reported previously. The copper position range is in agreement with Cu(0) chemical state; This is comforted by the lack of satellite excluding any Cu(II) contribution. Furthermore, the Auger CuLMM spectrum shows the peak position of kinetic energy at around 920 eV, illustrating that the main chemical state of Cu is in the zero valence.

The sample AuCu1:3/P25, after 15 minutes of photocatalytic reaction under UV light, was also characterized using XPS. The $Cu2p_{3/2}$ and $Cu2p_{1/2}$ peaks are found at 931.5 eV and 951.6 eV, and the Auger CuLMM peak is 921.9 eV (**Figure S11**), indicating the chemical status of Cu is still in zero valence. The unchanged violet color of the sample after reaction also confirmed the stabilization of the surface modified P25 with Au-Cu NPs in the photocatalytic reaction irradiated with UV light.

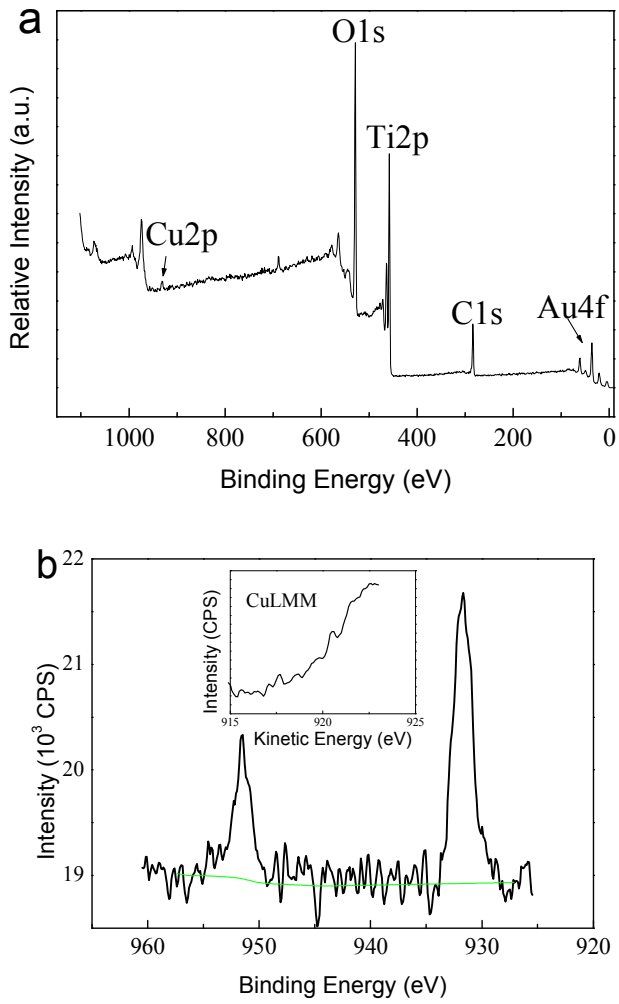

Figure 3(a) XPS survey spectrum and (b) Cu2p region of the XPS spectra of sample AuCu1:3/P25. The inset in b is Auger CuLMM spectrum of the sample.

3.2.5 DRS Analysis

Diffuse reflectance spectroscopy (DRS) is a useful method to characterize the electronic status of photocatalysts. **Figure 4a** shows the UV-Vis spectra of pristine and modified P25. P25 display a significant absorbance of UV light (λ is shorter than 400 nm), which is attributed to the large band gap (3.1 eV) of P25. All of the modified P25 display an absorbance in the visible region with respect to pure P25. The absorption maxima of Au/P25, AuCu1:1/P25 and AuCu1:3/P25 appeared at 552 nm, 565 nm and 563 nm, respectively. The intensity of the plasmon band (around 552 -563 nm depending on the sample) increases in intensity with the amount of gold. The absorption bands with maxima at various

wavelengths result in a violet color of the modified photocatalysts. For the sample Cu/P25, the absorbance maximum was found at 750 nm. It is well known that Au and Cu nanoparticles exhibit respectively a plasmon band with a maximum at ~520 nm and ~570 nm in aqueous solution. The absorption shift of the modified P25 photocatalysts is because the plasmon band is sensitive to the environment and to the stabilizer or the substrate. Because of the coupling between the metal nanoparticles and TiO_2 support having a high reflective index, the plasmon bands in case of Au/TiO_2 and Au-Cu/TiO_2 are red-shifted. However in case of Cu/TiO_2, the metal nanoclusters are very small and cannot exhibit a plasmon band because of their size. The wide absorption band in the visible and near infra-red region observed in this case could be due to inter-band transitions in the Cu clusters deposited on different phases and sites of TiO_2 and also with strong interaction with the support. It should also be pointed out there is a slight shift in band-gap transition to longer wavelengths from the DRS spectra of the modified photocatalysts. A similar effect was also previously observed with Pt- and Ag- modified TiO_2.[17, 18] This effect can be ascribed to a stronger stabilization of the conduction band of TiO_2 by the conduction band of the Au-Cu NPs compared to the stabilization of the valence band.

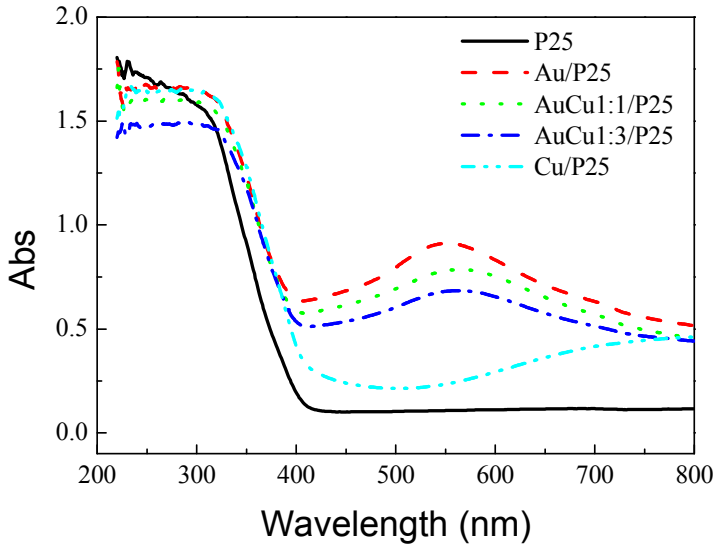

Figure 4 Diffuse reflectance UV-Vis spectra of the modified photocatalysts and pure P25.

3.3 Photocatalytic Tests

MO is a stable azo dye which is often taken as a model pollutant for photocatalytic tests. Its decomposition can be easily followed by UV-visible spectroscopy.[45-47] The photocatalytic activity of the modified P25 was investigated for the degradation of methyl orange (MO) under UV and visible irradiation. **Figure 5** shows the evolution of the absorption maximum (λ_{max} = 464 nm, the evolutions of the absorption spectra with irradiation time are shown in **Figure S12-15**) of MO with irradiation time under UV light. As seen, MO is very stable under UV illumination. The degradation is faster for the modified photocatalysts, except the monometallic Au modified P25, compared to the pristine P25. These photocatalytic reactions can be approximately regarded as first-order kinetics. The first order kinetics of MO photodegradation for the bare and modified P25 are shown in **Figure S16**. The rate constants were obtained by the linear fittings of $Ln(C_t/C_0)$ versus time *t*.

The rate constants of the reactions for MO photodegradation are presented in **Figure S17** and **Table S1**. Deposition of monometallic Au NPs on P25 by DPU method caused a decrease in the photoactivity compared to bare P25. In the case of modification with AuCu1:1 NPs, the photocatalytic efficiency doubled compared to that of the sample Au/P25. When the Cu/Au molar ratio increased to 3:1, the photocatalytic activity of AuCu1:3/P25 for MO degradation increased up to three times in comparison with pure P25. Modification with Cu leads to better enhancement of the photocatalytic activity compared to modification with Au.

Our results show that surface modification of P25 with monometallic Au NPs (by DPU method followed by radiolytic rduction) leads to lower photocatalytic activity under UV light; while this photocatalytic activity is enhanced in case of surface modification with Cu clusters. Bimetallic Au-Cu NPs modified P25 exhibit higher photoacatalytic activity under UV light compared to Cu modified P25: the highest activity is obtained with the Au/Cu ratio of 1:3.

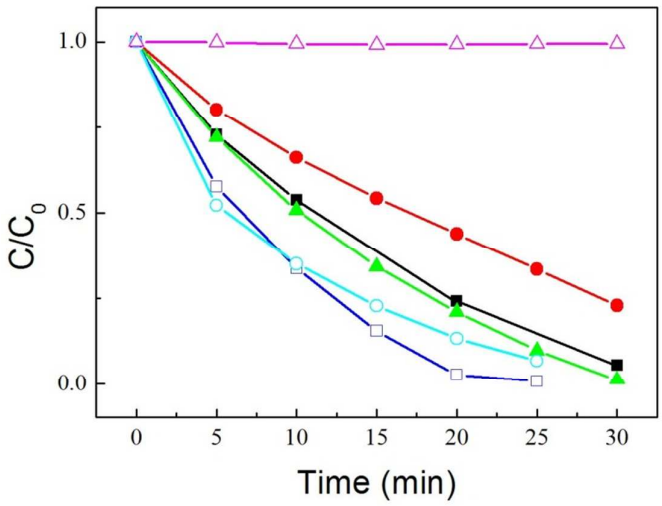

Figure 5 The time courses of relative MO concentration under UV illumination in the presence of P25 (filled square), Au/P25 (filled circle), AuCu1:1/P25 (filled triangle), AuCu1:3/P25 (open square), Cu/P25 (open circle), and no photocatalyst (open triangle).

For the photodegradation of MO under visible light, no degradation could be observed with the pristine or the Au, Cu, and Au-Cu modified P25. Contrary to rhodamine B (RhB), MO is not a photosensitive dye. According to the oxidation potential of RhB and the conduction band edge of TiO_2,[48, 49] the excited RhB molecules can transfer electrons into the CB of TiO_2, and themselves become cationic radicals which undergo further transformation.[50, 51] However, MO is a non-photosensitive dye.

The surface modification with Au, Cu, and Au-Cu NPs by DPU method does not improve the photocatalytic activity under visible light.

The modification of TiO_2 with plasmonic metal nanoparticles can induce a photocatalytic activity under visible light, but it is not always the case. Kowalska *et al.* studied the activity of Au particles (d_{Au} = 12−60 nm) loaded on TiO_2 for oxidation of 2-propanol under visible-light irradiation (λ > 450 nm) and they reported that rutile TiO_2 modified with larger Au particles show better photocatalytic activity.[52] The catalyst architecture is critical for the activity. The effect the photocatalytic activity in the visible seems to be very sensitive to the location on the nanoparticles on the surface and on their junction with the semiconductor, and it is still a matter of investigations. In case of Au on P25, it has been shown for example that this activity depends on the location of Au nanoparticles (diameters of <5 nm) on P25-TiO_2 and the plasmonic effect on photocatalysis is observed when Au nanoparticles are located at the

interface anatase/rutile.[53] Indeed, Au particles located at the anatase/rutile interface behave as the active sites, facilitating efficient e^- transfer toTiO_2 inducing an activity under visible light. In the case of TiO_2 modification with bimetallic NPs, Kowalska *et al*. also observed that Au-Ag modified TiO_2 are not active under visible light. In their work, co-deposition resulted in formation of bimetallic Au_{core}–Ag_{shell} structures, in which plasmonic photo-generated electrons sank into nearby second metal, instead of being transferred to conduction band of titania.[54]

3.4 Photoluminescence Spectra

Photoluminescence (PL) spectra of P25 and the modified TiO_2 are shown in **Figure 6**. PL emission is mainly due to the recombination of excited electrons and photogenerated holes in the semiconductor.[55] Thus, it is an effective mean to probe the recombination rate of the electron-hole pairs. In the spectra, the emission located at ~400 nm corresponds to the band-edge photoluminescence. The modified P25 exhibit lower PL intensities compared to pristine P25. Especially, the modification with Au-Cu bimetallic NPs with an Au/Cu ratio of 1:3 results in the lowest emission intensity. As it is described before, the sample AuCu1:3/P25 exhibits the highest photocatalytic acitivity among pure and modified P25 under UV irradiation. It is reasonable to expect that the decrease of the PL intensity may be beneficial the phtocatalytic activity.[56] The decrease in the electron-hole recombination is probably due to efficient electron scavenging by the metal nanoparticles. This scavenging effect has also been observed for Ag, Au, Cu, Pt and Au-Cu modified TiO_2.[17-19] The great improvement of photocatalytic efficiency is mainly due to more efficient separation of photo-induced electrons and holes in TiO_2. In the Cu modified samples, electron migrates from the semiconductor to Cu metal owing to the higher work function of copper.[57] Formation of Schottky barrier at the metal-semiconductor interface serves as an efficient electron trap preventing electron-hole recombination. The PL spectra indicate that Au associated with Cu is more efficient in electron scavenging compared to monometallic Au or Cu NPs. Nevertheless, monometallic Au modified P25 exhibits lower PL intensity, while its photocatalytic activity unexpectedly decreases with respect to pure P25. Two explanations are probably responsible for this phenomenon. First, Au NPs shelter part of the P25 surface decreasing the number of photo-induced electron-hole pairs. Consequently, the PL intensity is lower than that of

unmodified P25. Secondly, Au NPs are not as efficient as Au-Cu or Cu NPs in electron trapping.[19]

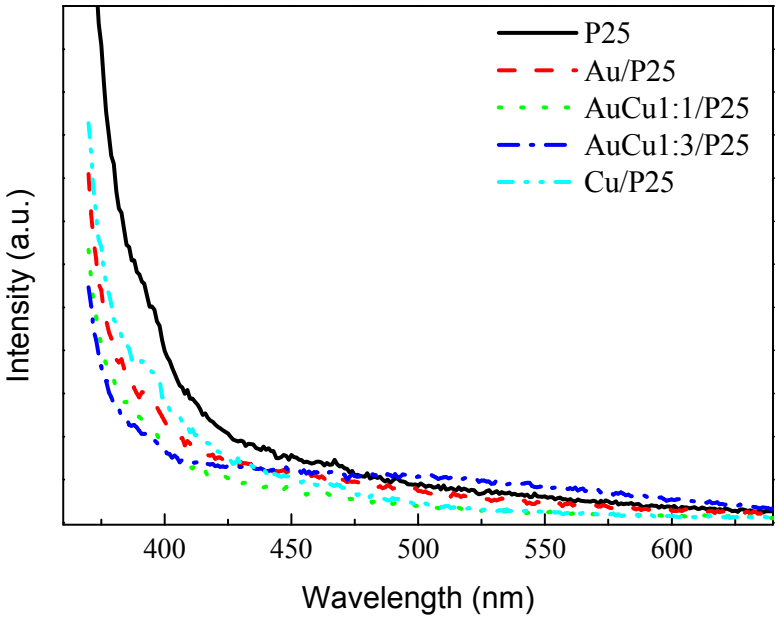

Figure 6 Photoluminescence spectra of the pristine and modified P25 photocatalysts with excitation at 325 nm.

4 Conclusions

Small Au-Cu NPs (~7 nm) were synthesized on the P25 support by radiolysis after deposition precipitation in the presence of urea. HR-TEM, HAADF-STEM, EDS, DRS, and XPS techniques have shown that the bimetallic Au-Cu NPs were nanoalloys. The modification of P25 with Au-Cu bimetallic NPs induces an enhancement in the photocatalytic activity under UV light. The highest UV photoactivity was obtained with modified P25 with Au-Cu NPs with ratio of 1:3. The supported Au-Cu NPs are stable in the photocatalytic reaction as confirmed by TEM and XPS techniques. The modification of P25 with Cu nanoclusters also induces an enhancement in the photocatalytic activity under UV light. The modification of TiO_2 with Cu and Au-Cu bimetallic NPs results in a decrease in the PL emission intensity due to less electron-hole recombination rates. Modification of P25 with Cu and Au-Cu nanoclusters induces a better separation of electrons and holes because the nanoclusters act as a sink for electrons, leading to an enhancement of the photocatalytic activity under UV light.

The two-step deposition precipitation with urea is efficient for depositing Au and Cu ions on P25, and it is applicable to deposit other metals (mono and bimetallic systems) on TiO_2 or on other substrates. These materials can also have applications in catalysis.

Acknowledgements:

The authors acknowledge Ewa Kowalska (Hokkaido University) for helpful discussions. The authors thank the China Scholarship Council for the funding support of joint PhD program and thank Jun Lv (Hefei University of Technology, China) for offering the photochemical reactor.

SI: Supporting Information

Description of the photocatalytic reactor, UV-vis spectra of the supernatants in the photocatalyst preparation, additional TEM images, N_2 adsorption isotherms, additional XPS spectra of AuCu1:3/P25, UV-vis spectra and first-order kinetics of MO photodegradation with the photocatalysts. This information is available free of charge via the Internet at http://www.rsc.org.

References

1 M. C. Hidalgo, J. J. Murcia, J. A. Navio and G. Colon, *Appl. Catal., A*, **2011,** *397*, 112.

2 T. Pasini, M. Piccinini, M. Blosi, R. Bonelli, S. Albonetti, N. Dimitratos, J. A. Lopez-Sanchez, M. Sankar, Q. He, C. J. Kiely, G. J. Hutchings and F. Cavani, *Green Chem.*, **2011,** *13*, 2091.

3 J. Zhang, Q. Xu, Z. Feng, M. Li and C. Li, *Angew. Chem. Int. Ed.*, **2008,** *47*, 1766.

4 O. T. Alaoui, A. Herissan, C. L. Quoc, M. M. Zekri, S. Sorgues, H. Remita and C. Colbeau-Justin, *J. Photochem. Photobiol. A*, **2012,** *242*, 34.

5 H. Wang, J. L. Faria, S. Dong and Y. Chang, *Mater. Sci. Eng., B*, **2012,** *177*, 913.

6 P. S. S. Kumar, M. R. Raj and S. Anandan, *Sol. Energy Mater. Sol. Cells*, **2010,** *94*, 1783.

7 S. T. Kochuveedu, D.-P. Kim and D. H. Kim, *J. Phys. Chem. C*, **2012,** *116*, 2500.

8 A. Veres, T. Rica, L. Janovak, M. Domok, N. Buzas, V. Zollmer, T. Seemann, A. Richardt and I. Dekany, *Catal. Today*, **2012,** *181*, 156.

9 A. Takai and P. V. Kamat, *ACS Nano*, **2011,** *5*, 7369.

10 D. Tsukamoto, Y. Shiraishi, Y. Sugano, S. Ichikawa, S. Tanaka and T. Hirai, *J. Am. Chem. Soc.*, **2012,** *134*, 6309.

11 J. Kim, D. Monllor-Satoca and W. Choi, *Energy Environ. Sci.*, **2012,** *5*, 7647.

12 P. Wongwisate, S. Chavadej, E. Gulari, T. Sreethawong and P. Rangsunvigit, *Desalination*, **2011,** *272*, 154.

13 V. Tiwari, J. Jiang, V. Sethi and P. Biswas, *Appl. Catal., A*, **2008,** *345*, 241.

14 C.-M. Wang, A. Heller and H. Gerischer, *J. Am. Chem. Soc.*, **1992,** *114*, 5230.

15 W. Choi, A. Termin and M. R. Hoffmann, *J. Phys. Chem.*, **1994,** *98*, 13669.

16 V. Subramanian, E. E. Wolf and P. V. Kamat, *J. Am. Chem. Soc.*, **2004,** *126*, 4943.

17 E. Grabowska, A. Zaleska, S. Sorgues, M. Kunst, A. Etcheberry, C. Colbeau-Justin and H. Remita, *J. Phys. Chem. C*, **2013,** *117*, 1955.

18 E. Kowalska, H. Remita, C. Colbeau-Justin, J. Hupka and J. Belloni, *J. Phys. Chem. C*, **2008,** *112*, 1124.

19 Z. Hai, N. E. Kolli, D. B. Uribe, P. Beaunier, M. Jose-Yacaman, A. Etcheberry, S. Sorgues, C. Colbeau-Justin, J. F. Chen and H. Remita, *J. Mater. Chem. A*, **2013,** *1*, 10829.

20 A. Eshaghi and A. Eshaghi, *Thin Solid Films*, **2011,** *520*, 1053.

21 N. Brodie-Linder, R. Besse, F. Audonnet, S. Lecaer, J. Deschamps, M. Imperor-Clerc and C. Alba-Simionesco, *Microporous Mesoporous Mater.*, **2010,** *132*, 518.

22 N. Brodie-Linder, S. Lecaer, M. S. Alam, J. P. Renault and C. Albe-Simionesco, *Phys. Chem. Chem. Phys.*, **2010,** *12*, 14188.

23 R. J. Chimentao, F. Medina, J. L. G. Fierro, J. Llorca, J. E. Sueiras, Y. Cesteros and P. Salagre, *J. Mol. Catal. A: Chem.*, **2007,** *274*, 159.

24 X. Liu, A. Wang, T. Zhang, D. Su and C. Mou, *Catal. Today*, **2011,** *160*, 103.

25 X. Liu, A. Wang, L. Li, T. Zhang, C. Mou and J.-F. Lee, *J. Catal.*, **2011,** *278*, 288.

26 A. Sandoval, C. Louis and R. Zanella, *Appl. Catal., B*, **2013,** *140-141*, 363.

27 N. E. Kolli, L. Delannoy and C. Louis, *J. Catal.*, **2013,** *297*, 79.

28 R. P. Doherty, J.-M. Krafft, C. Methivier, S. Casale, H. Remita, C. Louis and C. Thomas, *J. Catal.*, **2012,** *287*, 102.

29 M. Tominaga, Y. Taema and I. Taniguchi, *J. Electroanal. Chem.*, **2008,** *624*, 1.

30 M. Haruta, *Catal. Surv. Jpn.*, **1997,** *1*, 61.

31 S. Tsubota, D. a. H. Cunningham, Y. Bando and M. Haruta, *Stud. Surf. Sci. Catal.*, **1995,** *91*, 227.

32 A. Sandoval, A. Aguilar, C. Louis, A. Traverse and R. Zanella, *J. Catal.*, **2011,** *281*, 40.

33 R. Zanella, L. Delannoy and C. Louis, *Appl. Catal., A*, **2005,** *291*, 62.

34 R. Zanella, S. Giorgio, C. R. Henry and C. Louis, *J. Phys. Chem. B*, **2002,** *106*, 7634.

35 A. Hugon, L. Delannoy, J.-M. Krafft and C. Louis, *J. Phys. Chem. C*, **2010,** *114*, 10823.

36 F. Moreau, G. C. Bond, *Catal. Today*, **2007**, *122*, 260.

37 W. Abidi and H. Remita, *Recent Pat. Eng.*, **2010,** *4*, 170.

38 J. Belloni, M. Mostafavi, H. Remita, J. L. Marignier and M. O. Delcourt, *New J. Chem.*, **1998,** 1239.

39. S. Remita and H. Remita In: Wishart JF, Rao BSM, Eds. Recent Trends in Radiation Chemistry, Singapore: Word Scientific 2010: pp. 347-83.

40 R. J. Chimentao, F. Medina, J. L. G. Fierro, J. Llorca, J. E. Sueiras, Y. Cesteros and P. Salagre, J. Mol. Catal. A: Chem., **2007**, *274*, 159.

41 M. Tominaga, Y. Taema and I. Taniguchi, J. Electroanal. Chem., **2008**, *624*, 1.

42 S.W. Goh, A.N. Buckley, R.N. Lamb, R.A. Rosenberg, D. Moran, Geochim. Cosmochim. Acta 2006, 70, 2210.

43 S. Poulston, P.M. Parlett, P. Stone, M. Bowker, Surf. Interface Anal. 1996, 24, 811.

44 M.C. Biesinger, L.W.M. Lau, A.R. Gerson, R.St.C. Smart, Appl. Surf. Sci. 2010, 257, 887.

45 W. Wang, H. Cheng, B. Huang, X. Li, X. Qin, X. Zhang, Y. Dai, Inorg. Chem. **2014**, *53*, 4989.

46 P. Wang, Y. Xia, P. Wu, X. Wang, H. Yu, J. Yu, *J. Phys. Chem. C* **2014**, *118*, 8891.

47 C. Xing, Y. Zhang, Z. Wu, D. Jiang, M. Chen, *Dalton Trans.* **2014**, *43*, 2772.

48 K.-N. P. Kumar, J. Kumar and K. Keizer, *J. Am. Ceram. Soc.*, **1994,** *77*, 1396.

49 G. W. Scherer, *J. Am. Ceram. Soc.*, **1990,** *73*, 3.

50 T. Watanabe, T. Takizawa and K. Honda, *J. Phys. Chem.*, **1977,** *81*, 1845.

51 M. R. Hoffmann, S. T. Martin, W. Choi and D. W. Bahnemann, *Chem. Rev.*, **1995,** *95*, 69.

52 E. Kowalska, O. O. P. Mahaney, R. Abe, B. Ohtani, *Phys. Chem. Chem. Phys.* **2010**, *12*, 2344.

53 D. Tsukamoto, Y. Shiraishi, Y. Sugano, S. Ichikawa, S. Tanaka, T. Hirai, *J. Am. Chem. Soc.* **2012**, *134*, 6309

54 E. Kowalska, M. Janczarek, L. Rosa, S. Juodkazis, B. Ohtani, *Catal. Today* **2014**, *230*, 131.

55 P. Qu, J. Zhao, T. Shen and H. Hidaka, *J. Mol. Catal. A: Chem.*, **1998,** *129*, 257.

56 J. Tang, Y. Liu, H. Li, Z. Tan and D. Li, *Chem. Commun.*, **2013,** *49*, 5498.

57 S. Xu, J. Ng, X. Zhang, H. Bai and D. D. Sun, *Int. J. Hydrogen Energy*, **2010,** *35*, 5254.